Journal of the Brazilian Society of Mechanical Sciences and Engineering (2023) 45:4
https://doi.org/10.1007/s40430-022-03934-9

TECHNICAL PAPER

Tribological behavior and applicability analysis of cast iron and iron-based powder metallurgy for rolling piston rotary compressor under different applied loads

Shaopeng Ding[1,2] · Huijun Wei[1,2,3] · Ouxiang Yang[1,2] · Jun Wang[1,2] · Di Mu[2] · Yuanpei Hu[1,2]

Received: 17 June 2022 / Accepted: 26 November 2022 / Published online: 6 December 2022

Abstract
The tribological behaviors and applicability analysis of HT250 cast iron and iron-based powder metallurgy under different applied loads were compared experimentally. The friction coefficients and wear characteristics were measured with the changing operating load at a certain rotational speed by a ring-on-ring test rig. Results show that the tribological advantage is strongly dependent on the lubrication regime of frictional surfaces. The powder metallurgy presents better frictional performance in hydrodynamic lubrication when the applied load is less than 400 N. Still, with the applied load increasing beyond 400 N, the HT250 cast iron shows better frictional advantages in mixed lubrication. The Stribeck curve also shows the critical loads from hydrodynamic into mixed lubrication for the HT250 cast iron and powder metallurgy are about 300 N in present cases. Besides, with the increased applied load, the HT250 cast iron presents better anti-wear performance. The wear mechanism transforms from a significant abrasive feature to abrasive and oxidative wear.

Keywords Cast iron · Powder metallurgy · Friction coefficient · Wear performance · Lubrication regime

1 Introduction

Powder metallurgy (PM) and HT250 cast iron (HT250) have been widely applied as the bearing and diaphragm materials of rolling piston rotary compressors for air-conditioning. PM, due to the low cost, lightweight and high utilization, as well as the advantages of excellent lubrication properties, is adopted first in compressors. However, after a long run, the surface friction and wear limit the design and working life of tribological components. To this, HT250 is gradually applied to replace the PM owing to its friction-reducing performance and self-lubricating property. However, the potentiality of cost and processing of PM cannot be neglected. So the mechanism of friction and wear between two materials should be clear to compare their advantage and applicability.

PM and HT250 are typical metal materials, which have been studied on the friction and wear performance generally and separately. Currently, the main popularities focus on the influencing factor analysis such as matrix structure [1–3], graphite morphology [4], lubrication condition [5] and test pressure [6], and performance improvement by heat treatment [7], alloy element addition [8, 9], surface texture [10] and surface coating and treatment [11–14].

To the cast iron, Prasad [5, 15] systematically investigated the sliding wear properties under different oil lubrication to point out that, the gray cast iron performs better than that of the nodular one due to the harder and stronger matrix, the large surface area and greater thermal conductivity of flake graphite. Chen [16] researched the tribological performances of cast iron at high-speed dry sliding with different graphite morphologies, including flake, vermicular, and nodular. As the sliding speed increases, the wear rate increases, meanwhile, the friction coefficient decreases. The abrasive, oxidative and fatigue wear are the main wear mechanisms. Qin

Technical Editor: Daniel Onofre de Almeida Cruz.

✉ Huijun Wei
zgddsp@126.com

[1] State Key Laboratory of Air-Conditioning Equipment and System Energy Conservation, Zhuhai 519070, Guangdong, China

[2] Gree Electric Appliances, Inc. of Zhuhai, Zhuhai 519070, Guangdong, China

[3] Guangdong Key Laboratory of Refrigeration Equipment and Energy Conservation Technology, Zhuhai 519070, Guangdong, China

[17] conducted the pin-on-disk friction tests of steel-cast iron to study the wear mechanism. It is found that, with the increase in applied load, the wear mechanism transforms from adhesive and abrasive wear to oxidation and fatigue wear, even the severe spalling and plastic extrusion when the applied load increases to a certain value. Halim [18] fabricated the alumina coating by plasma spray to enhance tribological behavior, which showed the wear mass and friction coefficient could be reduced by 50% and 10%, respectively.

To the iron-based PM, Li [19] compared the dry sliding wear resistance between PM and cast iron by a ball-on-disk test. The friction coefficient and wear topography of PM are less than cast iron attributed to the evenly distributed lubricating graphite. The oxidation and stripping induced by plastic deformation are the primary wear mechanism. Ding [20] investigated the tribological differences between different densities and compositions. The carbon and copper contents are beneficial to reduce the friction coefficient by 27%. And with load increased, the wear mechanism transforms from abrasive to oxidative wear. To enhance strength and harden surface, Gulsoy [21] and Fang [22] improved wear performance by boron additions or boriding to find that the wear rate can be significantly decreased due to the increasing matrix hardness and density. And Liang [23] applied the amorphous alloy and surface sulfide to control the friction coefficient. The minimum value for the optimal sulfurizing formula can be reduced to 0.02.

PM and HT250 are the common materials widely used in rotary compressors and can be substituted mutually due to their similar mechanical properties. To the above descriptions, though the tribological behaviors of these two materials have been separately analyzed, the advantages comparison and applicability range on friction or wear properties under different operating conditions are not studied, which is the main topic in this article.

The main purpose of this study is to experimentally compare the friction and wear performances between the HT250 and the iron-based PM under different applied loads with oil lubrication. The friction coefficients were measured with the changing operating load at a rotational speed of 1500 r min^{-1} by a ring-on-ring test rig, which were used to analyze the lubrication regime. And the wear topographies and microstructure were also observed by scanning electron microscopy (SEM) and metalloscope analysis.

2 Experimental tests

2.1 Samples

A ring-on-ring friction couple consisting of the upper rotor and bottom stator is presented in Fig. 1. The upper rotor of JIS FC300 cast iron is rotated with a rotational speed of $\omega = 1500$ r min^{-1}. It originates from the rolling piston of the rotary compressor for air-conditioning (as shown in Fig. 2) with an outer diameter of 40 mm, an inner diameter of 27 mm, and a height of 24.2 mm. The static bottom stator is fabricated with two different materials, including the HT250 and the iron-based PM, respectively, which are used for the comparisons of friction and wear performance. The outer diameter is 54 mm, the inner diameter is 20 mm, and the height is 7 mm.

The HT250 material takes from a common bearing component of the rotary compressor and is machined to finally form bottom friction specimen.

To the iron-based PM material, 0.3% cutting agent is applied to improve cutting performance. After mixing of one hour, the mixed powder is molded and sintered under pressure of 500–600 Mpa and temperature of 1120 °C.

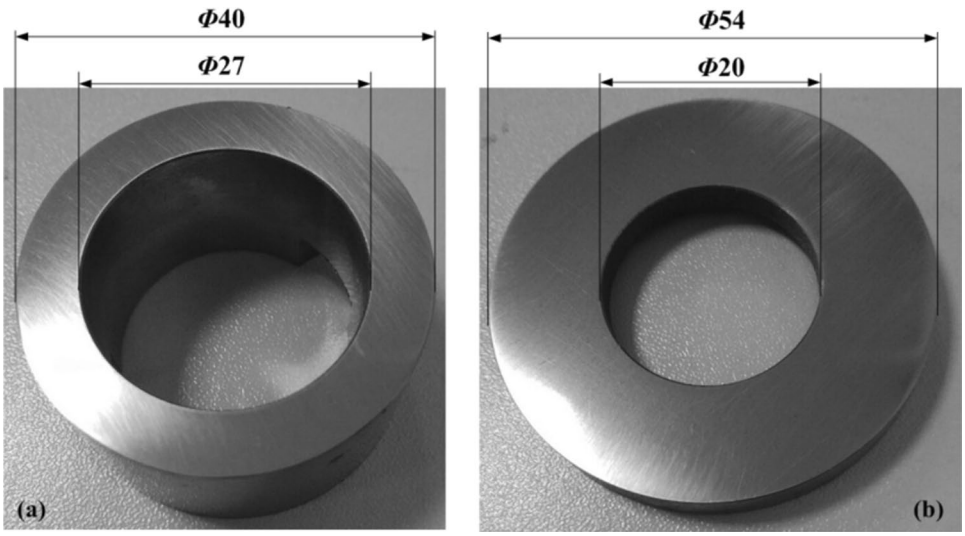

Fig. 1 Ring-on-ring friction couple

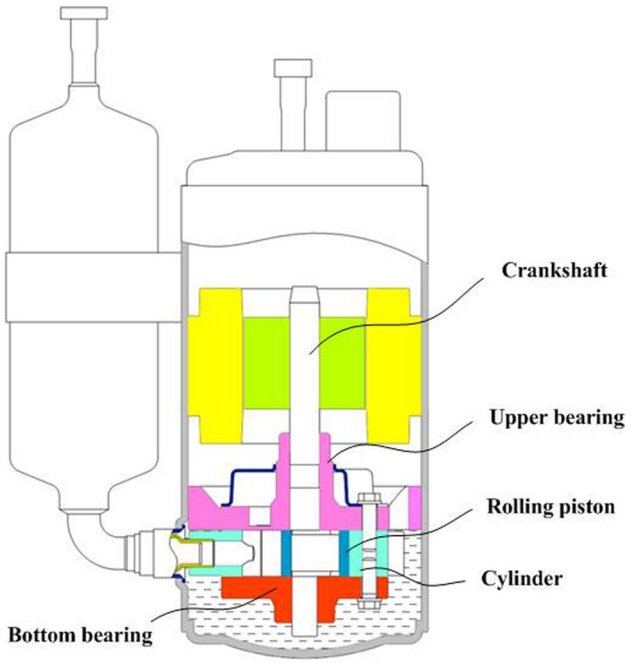

Fig. 2 Schematic of rotary compressor

Subsequently, the steam processing is carried out with 560 °C after 0.5 h heat preservation [20].

And all specimens are polished with a roughness of about $Ra < 0.2$ μm, then are cleaned in an ultrasonic cleaner with acetone and alcohol, and dried in an oven.

Compositional analysis is obtained with OES (Optical Emission Spectrometer) supported by Thermo Scientific ARL easySpark. The detailed characteristics of materials are given in Table 1. The hardness of multiple specimens is tested by a Brinell hardness tester with a steel ball diameter of 2.5 mm and applied force of 1839 N. Six measuring points evenly distributed along the circumference are selected for each specimen. Finally, the average value can be obtained as shown in Table 2 and Table 3.

The original topographies of the frictional surface on the bottom stator are measured on a white-light interfering 3D profile meter supported by BRUKER Contour GT-K, and that of the HT250 and PM are shown, respectively, in Fig. 3. The slight scars induced by abrasive wear during mechanical polishing can be observed, and the roughness of the frictional surfaces is controlled $Ra = 0.137$ μm for HT250 and 0.155 μm for PM.

Table 1 Characteristics of materials

Materials	Other ingredients except Fe / (%)						Density / (g cm^{-3})	Hardness / (HB)
	C	Cu	Si	Mn	Ni	Mo		
HT250	3.6	/	2.6	0.6	/	/	7.3	209.0
PM	0.9	1.2	/	/	2.0	1.3	6.7	179.6

Table 2 Hardness test of HT250 (HB)

Specimen numbers	Point 1#	Point 2#	Point 3#	Point 4#	Point 5#	Point 6#	Average value
No.1#	215.0	198.1	210.3	211.3	209.4	211.3	209.0
No.2#	212.2	211.3	213.0	209.4	212.3	205.8	
No.3#	197.3	203.2	205.8	212.2	215.7	216.0	
No.4#	199.5	204.9	210.3	207.6	198.9	205.8	
No.5#	213.2	210.0	212.1	206.3	217.0	215.2	

Table 3 Hardness test of powder metallurgy (HB)

Specimen numbers	Point 1#	Point 2#	Point 3#	Point 4#	Point 5#	Point 6#	Average value
No.1#	174.9	179.5	184.3	180.6	172.1	170.9	179.6
No.2#	182.2	185.3	180.3	179.4	182.3	185.1	
No.3#	177.2	187.3	185.2	175.8	175.7	184.0	
No.4#	170.3	179.5	180.9	182.6	177.9	182.8	
No.5#	173.2	180.6	176.3	182.1	177.1	183.2	

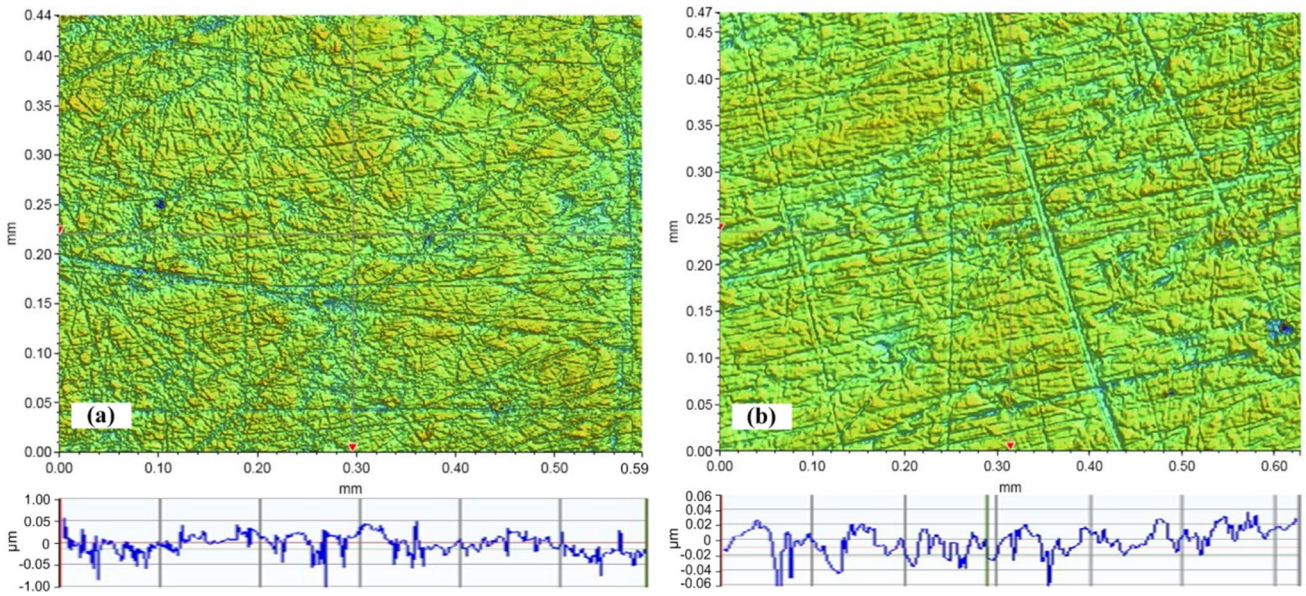

Fig. 3 Topographies of frictional surface: **a** HT250 and **b** PM

2.2 Testing parameters

Figure 4 demonstrates the MMW-1 tribometer with a ring-on-ring contact configuration used to compare the friction and wear properties of cast iron and powder metallurgy reference surfaces. The upper rotor is connected to a metallic holder driven by the motor with a rotational speed of 1500 r min^{-1}. The bottom stator is fixed on a tray by retaining pins to keep it static; and endured the applied load of F vertically. During running, the frictional surfaces are submerged into the lubrication (FV50S), and the friction coefficient is measured at least twice for each operating condition for one hour. After the testing, the wear topographies on frictional surfaces of the bottom stator are presented by SEM analysis (FEI Quanta250).

The test conditions and structural parameters are listed in Table 4.

Fig. 4 Schematic of test rig

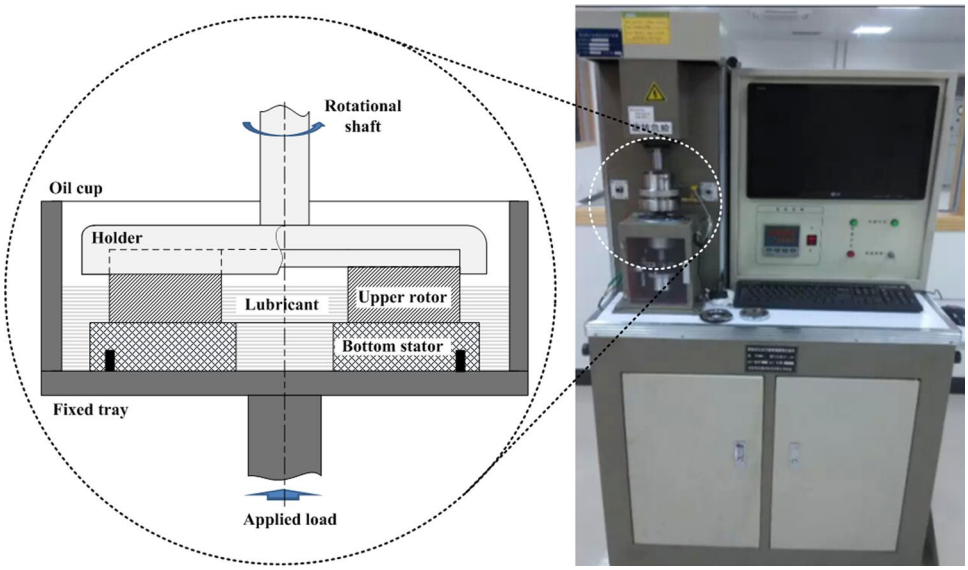

Table 4 Test conditions and structural parameters

Item	Symbol	Dimensions and data
Inner radius of frictional surface	r_i	13.50 mm
Outer radius of frictional surface	r_o	20.00 mm
Pressure in inner diameter	P_{in}	101,325 Pa
Pressure in outer diameter	P_{out}	101,325 Pa
Rotational speeds	ω	1500 r min^{-1}
Applied loads	F	0 ~ 800 N

3 Results and discussion

3.1 Friction coefficient

The influences of applied loads on the comparison of friction and wear performance between the HT250 and PM are studied. Figure 5 shows the friction coefficients of two different materials under $\omega = 1500$ r min^{-1} and $F = 400$ N with the increase in running time as one case.

The frictional curve can be divided into four stages: Firstly, during the start-up phase, the friction coefficient f drops sharply from a larger value of 0.1044 to 0.0365 for HT250 and from 0.1115 to 0.0441 for PM due to the transformation from static to dynamic friction coefficient. Secondly, during the acceleration phase, from 0 to 1500 r min^{-1}, the f increases rapidly due to the increasing friction force. Thirdly, during the running-in wear phase, the duration is 2600 s for HT250 and 3062 s for PM. The f decreases slowly. The PM presents a longer running-in time with a larger fluctuation amplitude of friction coefficient. Fourthly, during the steady wear phase, the f maintains steady approximately. In this case, finally, the f of HT250 can reach 0.0287, and PM, 0.0269.

In the author's last article [24], the tribological properties of HT250 have been presented. The comparison of friction curves with PM material under the same condition with the increase in applied load from 100 to 700 N is shown in Fig. 6. Note that each curve in this figure is obtained by a separate and independent test, then spliced into one picture.

As the F increases, the friction coefficients of two different materials present a similar tendency, namely first decrease slowly, then increase with a larger amplitude. To HT250 and PM, the transforming values of applied load are about 300 N with a minimum. The comparison between the two curves also shows that the PM has less friction coefficients than HT250 when F <400 N, but the differences between them gradually decrease. However, with the increase in applied load when F >400 N, the HT250 presents a less value and its advantage gradually enlarges.

The lubrication regime is discussed in Fig. 7 according to the Stribeck curves of the above two materials coming from the friction coefficient of the steady phase in Fig. 5. As the dimensionless parameter $\eta\omega/p$ decreases (right-to-left viewing), namely the applied load increases, for the HT250, the friction curve decreases firstly until a minimum of 0.0250 at $F = 300$ N, then increases with a larger amplitude. This can be concluded that the lubrication regime is transforming from hydrodynamic into mixed lubrication, and the critical

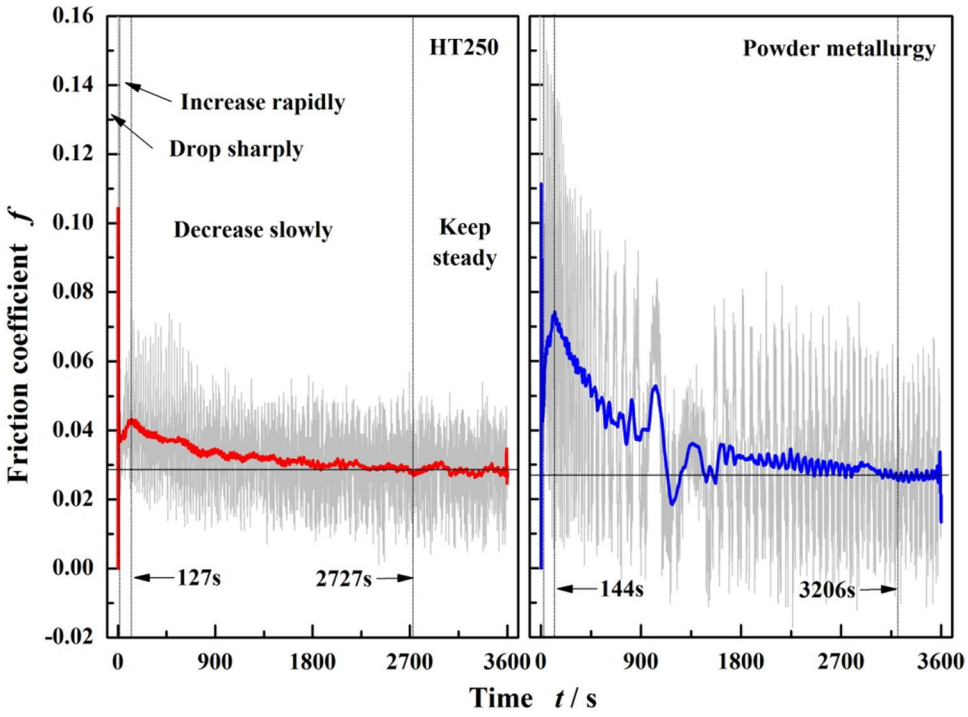

Fig. 5 Friction coefficients with the increase in time ($F = 400$ N)

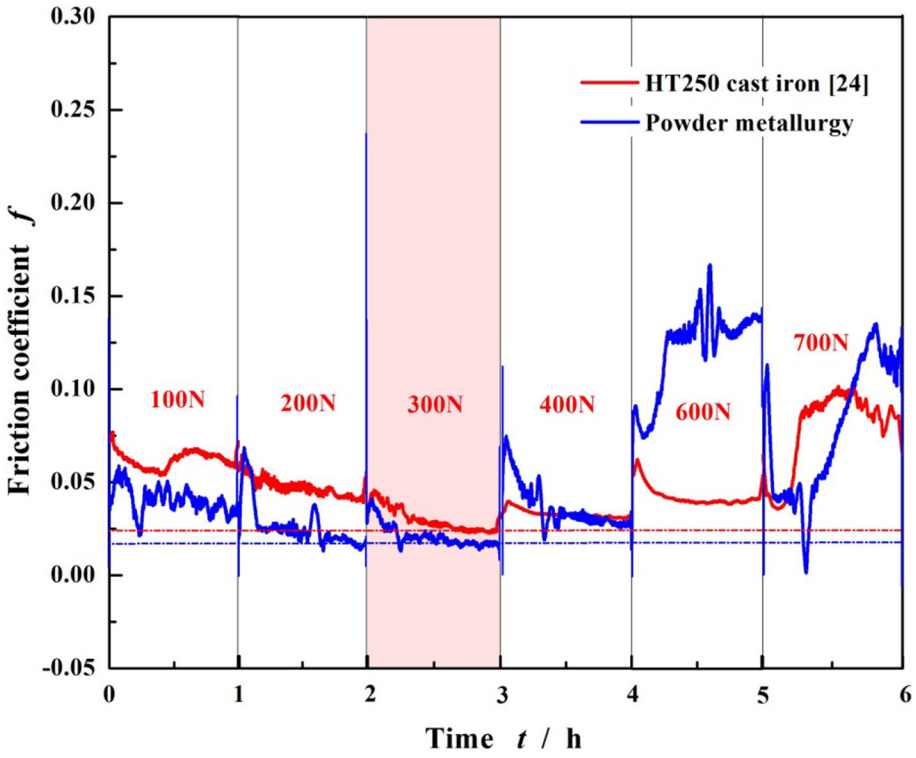

Fig. 6 Friction coefficients of different materials with the increase in time under different loads

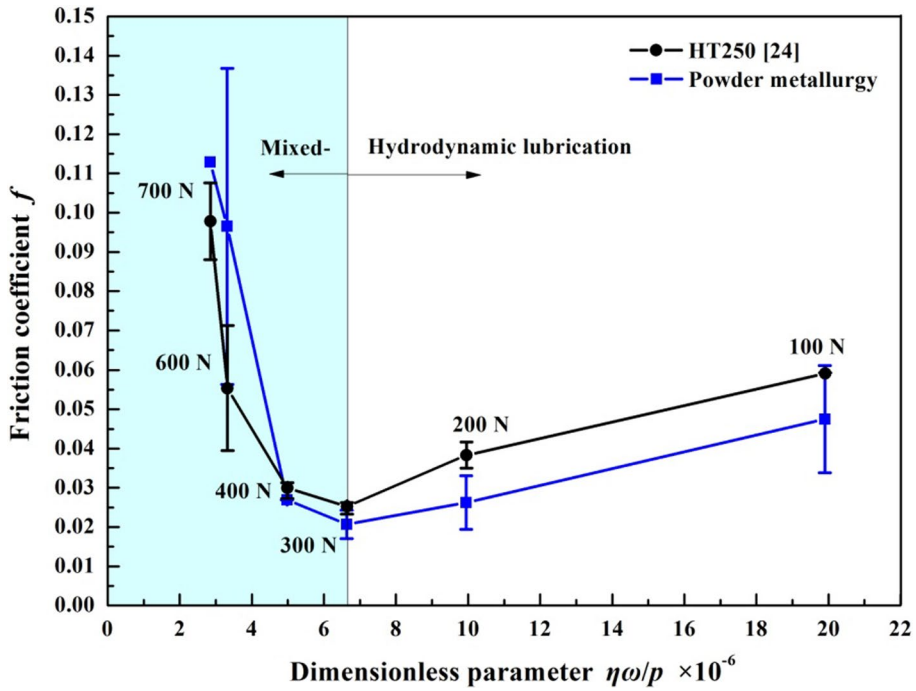

Fig. 7 Friction coefficients of different materials with the increase in dimensionless parameter under different loads (η is the viscosity of the lubricant, p is the load per unit area and ω is the rotational speed)

load is near 300 N. For the PM, the critical load is always about 300 N with $f = 0.0207$.

In general, by comparisons of friction curves, it is found that the PM presents better frictional performance in present cases when $F < 400$ N, with a decrease of 19.3%, 31.0%, 17.2%, and 9.2% at $F = 100$, 200, 300, and 400 N, respectively. But with the applied load increasing beyond 400 N, the HT250 shows better frictional advantages. To explain this phenomenon, the metallograph is obtained by metalloscope to analyze the microstructure, as shown in Fig. 8.

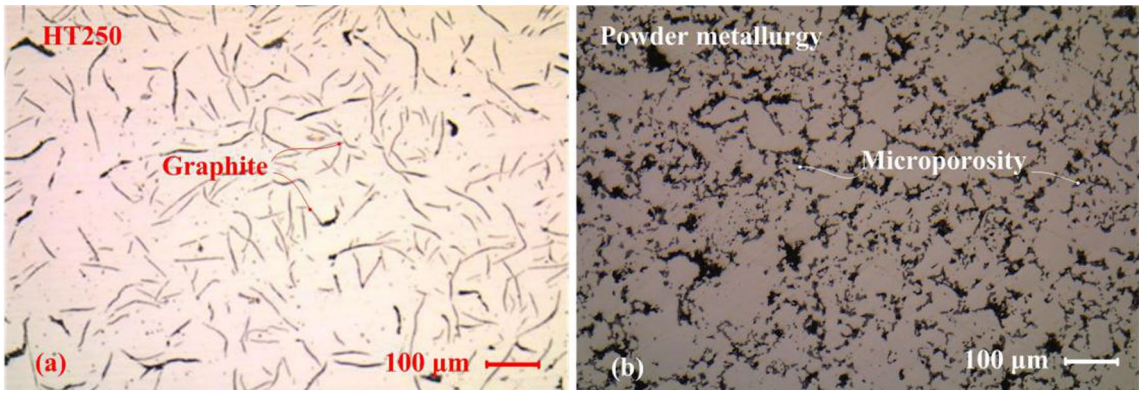

Fig. 8 Metallographic structures of HT250 and PM

By the metallograph, the PM presents a loose structure with microporosity, which is beneficial to preserve the lubricant when the applied load is lighter, thus maintaining full-film lubrication. But with the increased applied load, the weaker matrix strength and surface hardness (6.7 g cm^{-3} and 179.6 HB) compared with HT250 (7.3 g cm^{-3} and 209.0 HB) generates easily plastic deformation; as a result, this increases the surface friction and wear. However, to HT250 cast iron with more carbon composition, the increasing applied load forces graphite free from basis material to form graphite film with the self-lubricating property [25]. So when $F > 400$ N, the HT250 shows better frictional advantages and smaller frictional coefficients.

3.2 Wear performance

After frictional testing, the wear macrographs of the bottom specimens are shown in Figure 9. In general, the anti-wear performance of HT250 is better than that of powder metallurgy, especially for the higher applied load such as $F = 700$ N. With the increase in applied load, the wearing degree becomes more serious gradually for the two materials, and the significant wear scars and oxidative features (black wear area) can be found on frictional surfaces at $F = 700$ N.

Figure 10 demonstrates the wear topographies of two materials measured by SEM analysis. To $F = 200$ N in Fig. 10a and Fig. 10b, the slight scars induced by abrasive wear due to the original mechanical polishing can be observed, there is no other significant wear feature. To $F = 400$ N, the frictional surface of HT250 in Fig. 10c has significant scars induced by two-body abrasive wear compared with PM in Fig. 10d. So this can confirm the results in Figs. 7 and 9 that the PM presents a better anti-wear performance than the HT250 when $F < 400$ N.

However, to $F = 700$ N, the anti-wear property develops an opposite change. The HT250 presents the more

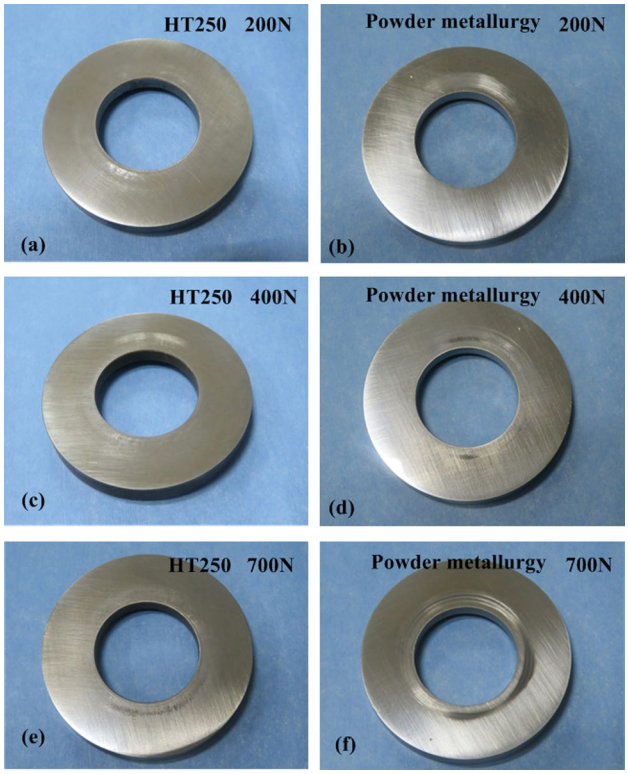

Fig. 9 Wear macrographs of bottom specimens: **a** HT250 at $F = 200$ N; **b** PM at $F = 200$ N; **c** HT250 at $F = 400$ N; **d** PM at $F = 400$ N; **e** HT250 at $F = 700$ N; **f** PM at $F = 700$ N

significant advantage of resisting surface wear. The original machining features and abrasive scars disappear after running the stable wear stage, as a result, the frictional interfaces become much smoother in Fig. 10e. The PM has an extensive plowing due to material loss induced by plastic extrusion, as a result, the loose microporosities are crushed without the preservation of lubricant. Besides, by the EDS analysis, the oxidation film in Fig. 10f can

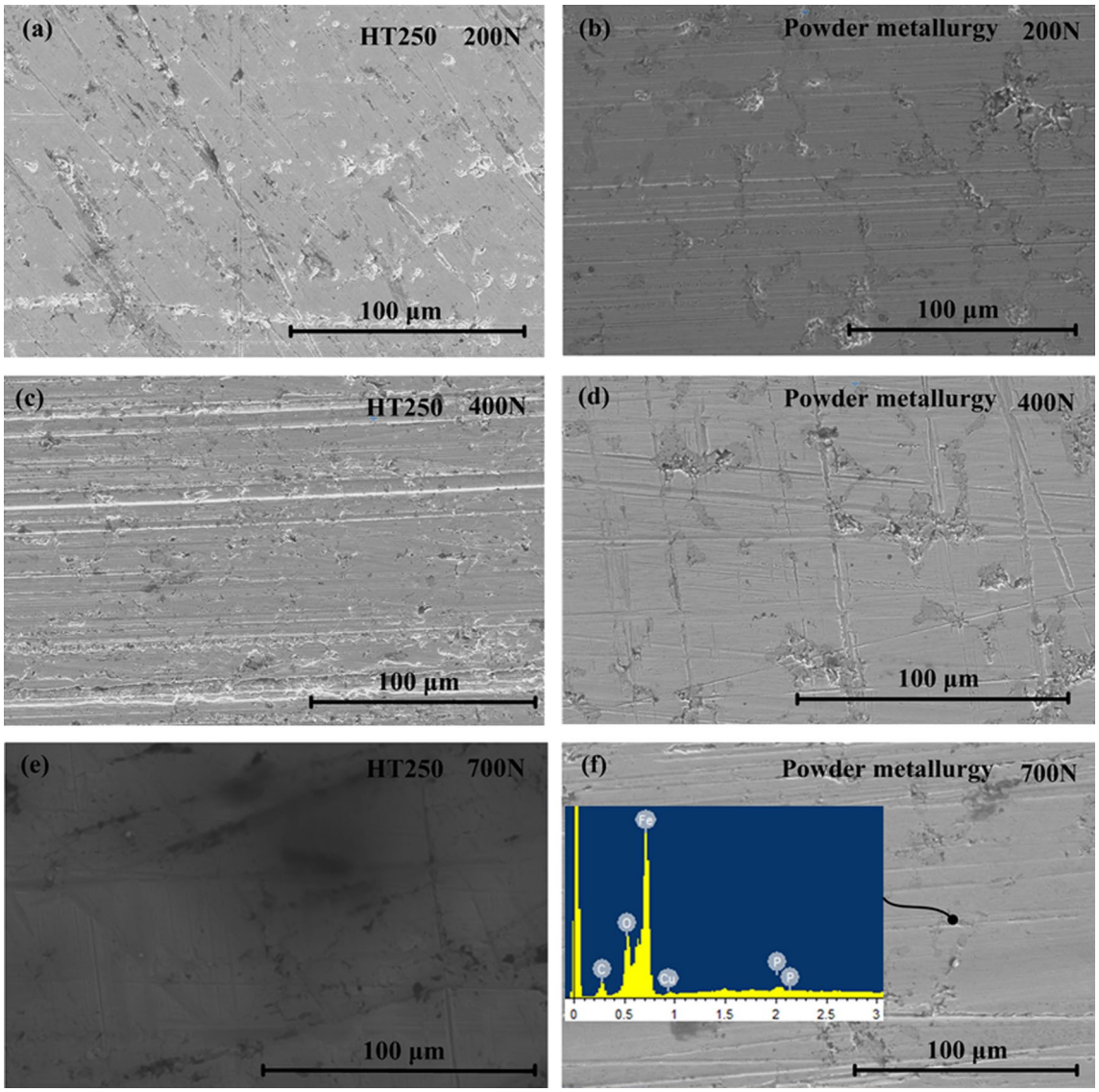

Fig. 10 Wear topographies of bottom specimens by SEM measuring: **a** HT250 at $F = 200$ N; **b** PM at $F = 200$ N; **c** HT250 at $F = 400$ N; **d** PM at $F = 400$ N; **e** HT250 at $F = 700$ N; **f** PM at $F = 700$ N

be found on the friction surfaces, which illustrating that the oxidative wear becomes the main wear feature at $F = 700$ N.

4 Conclusions

An experimental test was carried out for tribological comparisons and applicability analysis of cast iron and powder metallurgy under different applied loads for rolling piston rotary compressors. The friction coefficients and wear characteristics were measured. The following conclusions can be summarized:

(1) The tribological advantage of two materials is strongly dependent on the lubrication regime of frictional surfaces. In present cases, with the increase in applied load, the PM presents a better frictional performance when $F < 400$ N, but with the applied load increasing beyond 400 N, the HT250 shows better frictional advantages. The critical load from hydrodynamic into mixed lubrication for the HT250 and PM is about 300 N with the minimums.
(2) Two materials present different wear topography and wear mechanisms. With the increased applied load, the HT250 presents a better anti-wear performance, the abrasive wear is the dominant wear mechanism. But, for the PM material, the wear mechanism transforms from the significant abrasive feature to oxidative wear gradually.

(3) Compared with the HT250, the PM material used in this analysis is especially applicable in hydrodynamic lubrication or light load because of its loose structure to preserve the lubricant. Here, these two materials can be substituted mutually, and the PM can provide less friction coefficient and similar wear resistance. If applied in a heavy load or mixed lubrication, the material matrix of PM must be strengthened to enhance surface hardness and wear resistance to prevent microporosity be crushed. Or the HT250 becomes the preferred material.
(4) With the application of rotary compressors toward high speed and high load, PM material is suggested for strength enhancement by compositional change or addition, or other means. Besides, the rotational speed plays an important role in the transformation of the lubrication regime to affect the friction behavior and wear process, which needs further analysis.

Acknowledgments The research was financially supported by the Guangdong Basic and Applied Basic Research Foundation (No. 2020A1515011386, No. 2019A1515010787).

References

1. Collini L, Nicoletto G, Konecna R (2008) Microstructure and mechanical properties of pearlitic gray cast iron. Mater Sci Eng A 488:529–539
2. Zykova A, Kurzina I, Lychagin D (2014) Structural state, phase composition and mechanical properties of wear-resistant cast iron modified by ultrafine powders. Adv Mater Res 872:84–88
3. Ozkan D, Sulukan E (2018) The anti-wear efficiency of boron succinimide on engine cylinder liner and piston ring surfaces. J Braz Soc Mech Sci Eng 40:32
4. Zhang YZ, Chen Y, He R, Shen B (1993) Investigation of tribological properties of brake shoe materials-phosphorous cast irons with different graphite morphologies. Wear 166:179–186
5. Prasad BK (2007) Sliding wear response of cast iron as influenced by microstructural features and test condition. Mater Sci Eng A 456:373–385
6. Sun T, Song RB, Yang FQ, Wu CJ (2014) Wear behavior of bainite ductile cast iron under impact load. Int J Miner Metall Mater 21(9):871–877
7. Ghaderi AR, Nili Ahmadabadi M, Ghasemi HM (2003) Effect of graphite morphologies on the tribological behavior of austempered cast iron. Wear 255:410–416
8. Zumelzu E, Goyos I, Cabezas C, Opitz O, Parada A (2002) Wear and corrosion behaviour of high-chromium (14–30% Cr) cast iron alloys. J Mater Process Technol 128:250–255
9. Hu X, Chen X, Li YX (2013) Microstructure and mechanical properties of austempered high boron cast iron with modification and its mechanism discussion. Adv Mater Res 744:349–352
10. Lal R, Singh RC (2019) Investigations of tribodynamic characteristics of chrome steel pin against plain and textured surface cast iron discs in lubricated conditions. Math Probl Eng 16(4):560–568
11. Aal AA, Ibrahim KM, Hamid ZA (2006) Enhancement of wear resistance of ductile cast iron by Ni-SiC composite coating. Wear 260:1070–1075
12. Nakano M, Korenaga A, Korenaga A, Miyake K, Murakami T, Ando Y, Usami H, Sasaki S (2007) Applying micro-texture to cast iron surfaces to reduce the friction coefficient under lubricated conditions. Tribol Lett 28:131–137
13. Borgaonkar A, Syed I (2021) Friction and wear behaviour of composite MoS_2-TiO_2 coating material in dry sliding contact. J Braz Soc Mech Sci Eng 43:51
14. Feldshtein E, Devojno O, Wojciechowski S, Kardapolava M, Kasiakova I (2022) On the microstructure, microhardnessand wear behavior of gray cast iron surface layer after laser strengthening. Materials 15(3):1075
15. Prasad BK (2009) Sliding wear behaviour of a cast iron as affected by test environment and applied load. Ind Lubr Tribol 61(3):161–172
16. Chen Y, Shang-Guan B, Huang YY (2014) Research on tribological properties of cast iron at high-speed dry sliding condition. Adv Mater Res 936:2063–2067
17. Qin SD, Wang SQ, Chen NL (2011) Wear behaviors and mechanism of gray cast iron under dry sliding condition. Heat Treat Met 36(6):73–78
18. Halim Z, Ahmad N, Hanapi MF, Zainal MN (2021) Rapid surface treatment of grey cast iron for reduction of friction and wear by alumina coating using gas tunnel plasma spray. Mater Chem Phys 260:124134
19. Li XR, Liu JB, Xiong J, Yang L, Gou QS, Song XY, Guo ZX, Hua T, Liang MX (2020) Wear and corrosion resistant Mn-doped austenitic cast iron prepared by powder metallurgy method. J Mater Res Technol 9(3):6376–6385
20. Ding SP, Xu J, Shi ZL, Yang OX, Deng LY, Liu P (2021) Influence of different densities and compositions on friction and wear behaviors of powder metallurgy. Lubr Eng 46(9):105–112
21. Gulsoy HO, Bilici MK, Bozkurt Y, Salman S (2007) Enhancing the wear properties of iron based powder metallurgy alloys by boron additions. Mater Design 28:2255–2259
22. Fang HM, Xu F (2020) Research on properties of Fe-based powder metallurgy material strengthened by boriding. Strength Mater+ 52(4):621–626
23. Liang XJ, Ji HX (2022) Reliability of friction and wear characteristics of surface-strengthened iron-based powder metallurgy materials. Integr Ferroelectr 229(1):190–209
24. Ding SP, Xu J, Liu PF, Shi ZL, Yang OX, Hu YP (2021) Geometric influence on friction and wear performance of cast iron with a micro-dimpled surface. Results Eng 9:100211
25. Zhang BF, Ma X, Lu XQ, Song Y, Shi YF, Fu YD (2022) Effect of cylinder liner cast iron microstructure on friction and wear process. Mater Sci Tech-Lond. https://doi.org/10.1080/02670836.2022.2130519